



Collapse modeling of thin-walled cylinder with measured imperfections

Xi Peng¹, Dehui Lin², Saravanan Subramanian³,
Anil Pervizaj⁴, Andrew T. Myers⁵, Benjamin W. Schafer⁶

Abstract

The objective of this paper is to report on the modeling protocols and application of high-resolution laser scanning in the nonlinear collapse analysis predictions of thin-walled steel tubes in flexure by shell finite elements. The benchmark tubes under study are motivated by fabrication and loading details consistent with wind turbine support towers. Two 1m diameter tubes of varying slenderness fabricated in a traditional can-welding procedure, and tested in flexure with heavy end platens are utilized as benchmarks. The fabricated specimens were laser-scanned prior to testing. Shell finite element simulations of pure bending of the tested tubes are conducted in both ABAQUS and ANSYS to investigate solver independency. Linear buckling analysis (LBA), material nonlinear analysis (MNA), and geometrically and materially nonlinear analysis with imperfections included (GMNIA) are performed. Three types of imperfections are imposed in the shell finite element model: first eigenmode-affine patterns, weld depression patterns, and scanned imperfections. In terms of material behavior, two proportional limits are considered in the GMNIA analysis to study the influence of material modeling on the response of tube. Simulation results are compared with experimental data. This research is intended to help establish (a) direct connections between measured imperfections, imperfection quality class, and predicted strength, and (b) clear guidance on the use of nonlinear collapse analysis to establish the strength of thin-walled steel tubes for use in creating more efficient tower designs.

1. Introduction

In the pursuit of sustainable and renewable energy sources, wind power has emerged as a key contributor. In the past few decades, the levelized cost of the energy produced by individual wind turbines has decreased markedly, while the size and scale of those same turbines has increased (Lantz et al 2019). Notably, tower heights have increased, to accommodate the ever larger swept areas, and to chase higher steadier wind. Wind turbine support towers are commonly thin-walled steel cylinders manufactured by can-welding, consisting of rolling steel plates into cylinders,

¹ Graduate Research Assistant, Johns Hopkins University, <xpeng26@jh.edu>

² Ph.D. Candidate, Northeastern University, <lin.deh@northeastern.edu>

³ Assistant Lead Engineer, Vestas, India, <srsba@vestas.com>

⁴ Lead Engineer, Vestas, Denmark, <anpij@vestas.com>

⁵ Professor, Northeastern University, <an.myers@northeastern.edu>

⁶ Professor, Johns Hopkins University, <schafer@jhu.edu>

seam-welding them into cans, and stacking and circumferentially welding the cans to one another to form a section of a tower. This process inevitably introduces imperfections, which notably influence the structural capacity of the tower.

The effect of imperfections on the structural capacity of thin-walled cylindrical shells has been continuously investigated by researchers over decades and consideration of imperfections is an integral part of their design. Eurocode 3 Part 1-6 (i.e., EC3-1-6: CEN 2007) provides the world's most comprehensive provisions for the design of civil shell structures and is utilized in wind turbine support tower design. EC3-1-6 classifies shell structures into Class A (excellent), Class B (high), and Class C (normal) based on measurement of imperfection magnitudes, and this fabrication quality parameter is used in the stress-based design approach for strength reduction. EC3-1-6 also covers the utilization of more advanced computational methods in the shell design, including linear buckling analysis (LBA), material nonlinear analysis (MNA), and geometrically and materially nonlinear analysis with imperfections (GMNIA). GMNIA explicitly requires the introduction of imperfections, with eigenmode-affine patterns, weld depression patterns, and physically scanned imperfection patterns all previously considered in simulations of others (e.g., Rotter and Schmidt. 2013, Rotter and Teng. 1989, Mahmoud 2017). Several of the authors have been involved in previous studies focused on structural performance of tubes relevant to wind turbine support towers, including the experimental and modeling work conducted on tapered spirally-welded tubes subject to bending (Mahmoud et al. 2016, Mahmoud et al. 2018, Jay et al. 2016a, Jay et al. 2016b). Sadowski et al. (2023) provided a comprehensive assessment of current design rules for tubes. Existing work on can-welded tubes includes studies on compression (Berry et al. 2000) and bending (Wang et al. 2020). The commercial software ABAQUS is the most commonly used finite element solver in published research on wind turbine towers (Sadowski et al. 2023, Sadowski and Seidel. 2023). However, existing studies rarely focus on sensitivity of the collapse solution to choice of software and solvers, nor applying high-resolution laser scanning in the simulation of nonlinear flexural buckling of thin-walled steel tubes, nor studies the effect of material modeling and the choice of proportional limit, all relevant to wind turbine support tower simulation.

To address this knowledge gap, shell finite element GMNIA collapse simulations of two recently tested thin-walled tubes with different slenderness are conducted. Three types of geometric imperfections: first eigenmode-affine, weld depression, and scanned imperfections are considered in the simulations. The effect of material proportional limit is also investigated by considering limits of $1.0 f_y$ and $0.6 f_y$ in the simulated material stress-strain response. In addition, and unique to this study, the GMNIA simulations are performed in two different commonly used modeling software: ABAQUS and ANSYS. All results are compared with experiments recently conducted in the STRESS laboratory at Northeastern University (Lin et al. 2024).

2. Geometry of the thin-walled tubes

The geometry of a thin-walled cylinder can be characterized by diameter (D), thickness (t), and length (L). The modeling protocols investigated in this paper are validated against two large-scale flexural tests, identified as CW-158-1 and CW-315-3, from an ongoing experimental program. Summary information is provided in Table 1 including the D/t ratio of the two tubes, which is also the number aligns identified in the specimen nomenclature. Note, "CW" refers to can-welded, and the final number identifies nominally identical replicants in the test series. A schematic diagram

of the cans that comprise the thin-walled cylinder is shown in Fig. 1. Specimens are welded with 3 “full” cans with a length of 825.5 mm and 2 “half” cans at the ends with a length of 412.75 mm.

Table 1: Summary of geometry of specimens

Specimens	D (mm)	t (mm)	L (mm)	D/t
CW-158-1	1003	6.35	3302	158
CW-315-3	1003	3.175	3302	315

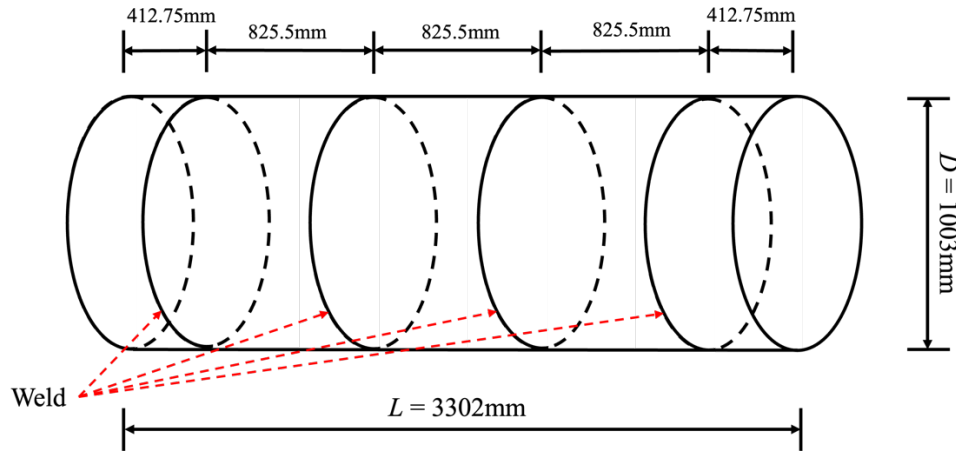


Figure 1: Schematic diagram of the thin-walled cylinder

3. Experimental summary

The experiments utilized herein are part of a larger test series being conducted by a subset of the authors at the STRESS lab at Northeastern University (Lin et al. 2024). Prior to testing all specimen geometry and imperfections are recorded using a high-resolution laser scanner. Maximum measured imperfections and preliminarily assigned quality class for two specimens are provided in Table 2. For specimen CW-158-1, out of roundness, eccentricity, and dimple imperfections for the weld meets the requirement of class A in EC 3-1-6, but dimple imperfections for longitudinal and circumferential are quality class B, so the overall specimen quality class is B. The specimen quality class for CW-315-3 is C.

Fig. 2(a) provides a picture of the test rig and Fig. 2(b) an annotated schematic of the test rig. The rig applies pure moment to the ends of the cylinder through two hydraulic actuators. The primary actuator is contracted in displacement control, and the secondary actuator is extended in load control creating equal and opposite forces. The specimens are welded to substantial endplates, which are in turn connected to cross beams of the testing rig by bolts. The “left” cross beam is pinned and the “right” cross beam is pinned into a slotted hole that allows movement in the longitudinal direction (again ensuring no net compression or tension). Before the actual loading, a small amplitude load cycle is applied to estimate the frictional moment. After loading begins, the test is regularly stopped for laser-scanning of the compression zone of the tube. The test is complete when the total rotation of the two ends of the specimen reaches 2 degrees, or other limit states occur. The complete test series is still ongoing as of this writing.

Table 2: Measurements of the maximum imperfection metrics and associated quality classes (QC) in EN 1993-1-6

Specimen	EN 1993-1-6 Imperfections										Spec. QC
	Out-of-roundness		Eccentricity		Dimple						
	$U_{r,max}$	QC	$U_{e,max}$	QC	Longitudinal		Circumferential		Weld		
					$U_{0x,max}$	QC	$U_{0\theta,max}$	QC	$U_{0w,max}$	QC	
CW-158-1	0.0065	A	0.0504	A	0.0061	B	0.0088	B	0.0057	A	B
CW-315-3	0.0161	C	0.2251	C	0.0134	C	0.0160	C	0.0095	B	C

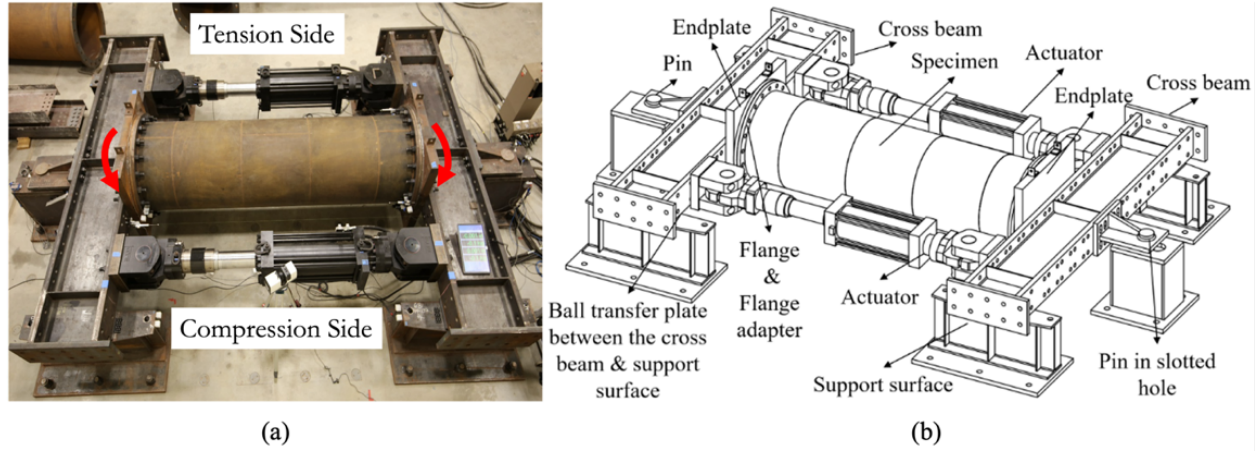


Figure 2: (a) Picture of test rig; (b) Schematic diagram of test rig (Lin et al 2024)

4. Finite element modeling

4.1 Features of numerical model

Finite element analysis of specimen CW-158-1 and CW-315-3, including LBA, MNA, and GMNIA, are conducted in both ABAQUS and ANSYS. Shell elements are selected for the finite element models, and S4R shell element is chosen in ABAQUS while SHELL 181 element is used in ANSYS. Mesh size of all numerical models is selected to be no larger than $0.25\sqrt{Rt}$ and element aspect ratio is set to 1:1 as recommended by Mahmoud et al. (2018). This results in a physical mesh with 14 mm long elements in specimen CW-158-1 and 9 mm for CW-315-3. For boundary conditions of the model the two ends are coupled to corresponding reference points in the end sections as shown in Fig. 3, utilizing MPC-beam constraints in ABAQUS, and constraint equation rigid (CERig) in ANSYS. Loading in the model consists of moment about the y axis. Nodal coordinates and boundary conditions of the reference points are shown in Table 3. Consistent with the test setup, at the reference points transverse displacement and torsional rotation are restrained. At reference point 1, longitudinal displacement is also restrained.

Table 3: Nodal coordinates and boundary conditions of numerical model

Reference points	Nodal Coordinates			Degree of Freedom					
	x (mm)	y (mm)	z (mm)	U1	U2	U3	UR1	UR2	UR3
RP-1	0	0	3302	X	X	X			X
RP-2	0	0	0	X	X				X

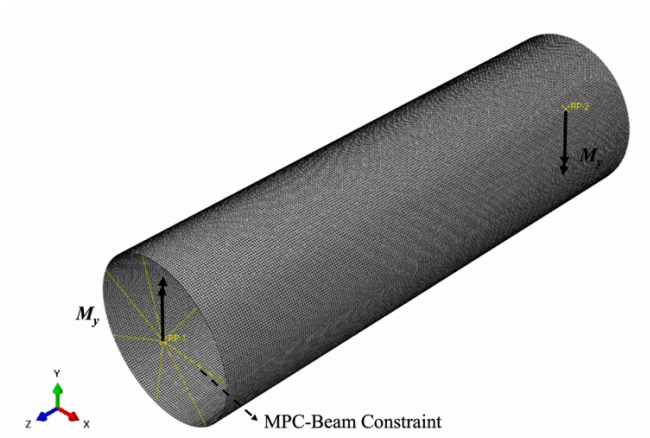


Figure 3: Features of numerical model

4.2 Material properties

Material (σ, ϵ) properties in the model are based on tensile coupon tests of the specimens. However, elastic modulus is set to 200 GPa and Poisson's ratio to 0.3 in all models. Plasticity is modeled with von Mises yield criteria, associated flow, and isotropic hardening that is matched with true stress-strain curves measured for each specimen in both ABAQUS and ANSYS. Material properties for engineering yield stress, engineering ultimate stress, and engineering ultimate strain are shown in Table 4 and stress-strain curves for the coupon tests and selected matching curves are provided in Fig. 4. For the material response provided to the model two different assumptions are considered: one where the proportional limit is set at $1.0f_y$ consistent with a sharp-yielding steel and one where it is set at $0.6f_y$ consistent with a more gradual yielding steel. As Fig. 4 shows, the response assuming the lower proportional limit more precisely captures the elastic-plastic transition, but for strains greater than 0.5% differences are minimal. For both ABAQUS and ANSYS, it is assumed engineering stress and strain obtained from coupon test measurement can be converted into true stress and strain by the following formulas:

$$\epsilon_{true} = \log(1 + \epsilon_{eng}) \quad (1)$$

$$\sigma_{true} = \sigma_{eng}(1 + \epsilon_{eng}) \quad (2)$$

Table 4: Summary of material properties: Engineering Yield stress (f_y), Ultimate Stress (f_u), Ultimate Strain (ϵ_u)

Specimens	f_y (MPa)	f_u (MPa)	ϵ_u
CW-158-1	409	480	0.157
CW-315-3	412	488	0.179

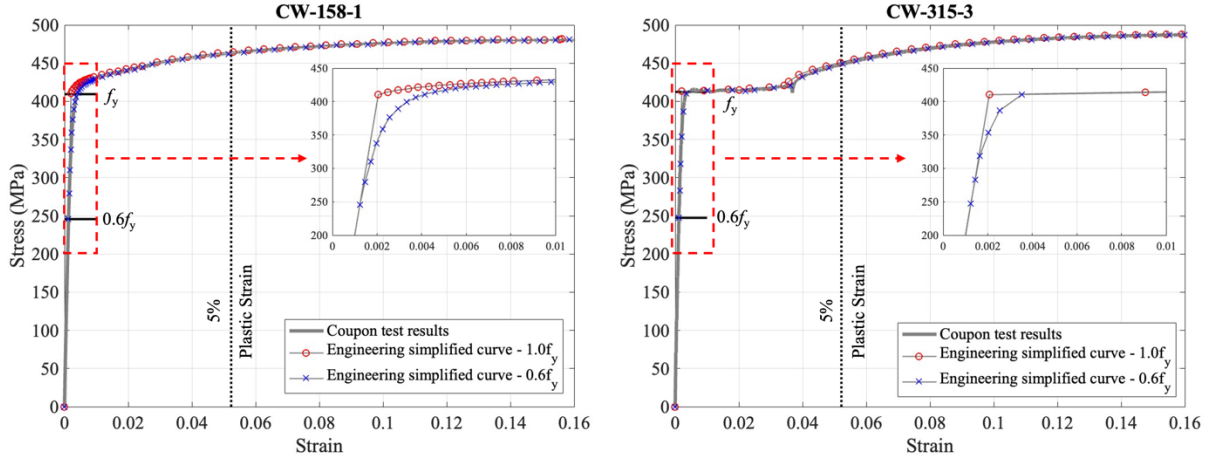


Figure 4: Coupon test results for all specimens

4.3 Imperfections

Geometric imperfections are modeled assuming three possible patterns: first eigenmode-affine, weld depression, and scanned imperfections. For the eigenmode and weld depression imperfections the magnitude is associated with the three quality classes in EC3-1-6. Note, as a baseline, geometric and material nonlinear analysis (GMNA) for the perfect tube is also conducted for comparison with the GMNIA models.

First eigenmode-affine patterns (See Fig. 5 (a)) are commonly recommended in numerical modeling, including by EC3-1-6, “unless a more unfavorable pattern is considered” (CEN 2007). The magnitude of first eigenmode imperfections ($\Delta w_{0,eq1}$) are calculated based on a reference gauge length (l_g) and values for dimple imperfection amplitude parameters (U_{n1}), where the imperfection magnitude $\delta_0 = l_g U_{n1}$, and U_{n1} corresponds to a specific quality class. The gauge length l_g is assumed equal to $l_{gx} = 4\sqrt{Rt}$, which represents the gauge length in the meridional direction (CEN 2007). Imperfection magnitudes for each specimen are shown in Table 5, and vary from 1.6 mm to 5.63 mm.

The weld depression imperfection pattern assumes the only important imperfections exist at the circumferential can welds (See Fig. 5 (b)(c)) and have been shown to be critically influential in flexural collapses (Wang, J. et al (2020)). For the exact pattern, the type A weld depression profile suggested by Rotter and Teng (1989) is employed as provided in Eq. 3:

$$\delta(x) = \delta_0 e^{-\frac{\pi}{\lambda}|x-x_w|} \left(\cos\left(\frac{\pi}{\lambda}|x-x_w|\right) + \zeta \sin\left(\frac{\pi}{\lambda}|x-x_w|\right) \right) \quad (3)$$

where x_w denotes the longitudinal location of central line of weld and λ is the linear meridional bending half wavelength ($\lambda = 2.44\sqrt{Rt}$). If $\zeta = 1$, the profile is the Type A weld depression. If $\zeta = 0$, the profile is the Type B weld depression. The magnitude of the weld depression, δ_0 , is calculated by considering the gauge length (l_g) and values for dimple imperfection amplitude parameters (U_{n1}), where $\delta_0 = l_g U_{n1}$. The gauge length (l_g) is calculated assuming $l_g = l_{gw} = \min(25t, 500)$, which is the gauge length across a weld in the circumferential direction per EC3-

1-6. Values of the weld depression imperfection magnitudes are provided in Table 5 and vary from $0.25t$ (Class A) up to $0.625t$ (Class C).

The scanned imperfections (See Fig. 6) are included in the model as imperfections by adjusting the radial distance of the node points to best match the closest point in the scanned data. Use of the closest point algorithm works well because the scanned data has a resolution of 1mm which is much higher than the finite element mesh node points. However, gaps exist in the scanned data around the weld zone due to removal of the weld bead surface from the scanned points. To address this a Fourier series is introduced for fitting the imperfection surface. The coordinate system of the tube used for the Fourier series approximation is shown in Fig. 7, where global coordinate system (X, Y, Z) and local coordinate system (x, y, z) are all included. For the local coordinate system, x is the circumferential direction (unit: rad), y is the longitudinal direction, and z is the radial direction. (For other symbols in Fig. 7, R denotes radius, t thickness, and l length.) The chosen series approximation $I(x,y)$ is set as follows:

$$I(x, y) = \left[a_0 + \sum_{i=1}^p (a_{s,i} \sin(ix) + a_{c,i} \cos(ix)) \right] \cdot \left[b_0 + b_1 \frac{y}{l} + \sum_{j=1}^q (b_{s,j} \sin(\frac{j\pi y}{l})) \right] \quad (4)$$

By expanding and substituting terms in Eq. 4, a formula with total number of $n = (2p + 1)(q + 2)$ terms with unknown coefficients can be obtained. The number of terms used in the left and right Fourier series is selected in part based on the gauge length of the tube as follows:

$$l_g = \min(l_{gx}, l_{g\theta}, l_{gw}) = \min(4\sqrt{Rt}, \min(2.3\sqrt[4]{L^2Rt}, R), \min(25t, 500)) \quad (5)$$

where the value of p and q can be calculated by $p = 2.5\pi R/l_g$, $q = 1.5 L/l_g$. Assume we have scanned imperfection data at m locations ($m > n$), an overdetermined linear system with number of equations being m and number of unknown coefficients being n can be formed. To solve this overdetermined linear system, MATLAB is employed (i.e., operator ‘/’ is used), which provides a solution with minimized error. In this case, $n = 4212$ for specimen CW-158-1, and $n = 8395$ for specimen CW-315-3, and $m = 1000000$ for two specimens. Scanned imperfections with the zone of the weld bead filled with data generated by the fitted Fourier series are provided in Fig. 8.

Table 5: Magnitude of the Maximum Imperfection Considered in the GMNIA Models for Specimens

Specimen	1 st Eigenmode-affine pattern			Weld depression pattern		
	$\Delta w_{0,eq1}$ (mm)			δ_0 (mm)		
	Imperfection classes in EC3			Imperfection classes in EC3		
	A	B	C	A	B	C
CW-158-1	2.25	3.61	5.63	1.59	2.54	3.97
CW-315-3	1.60	2.55	3.99	0.79	1.27	1.98

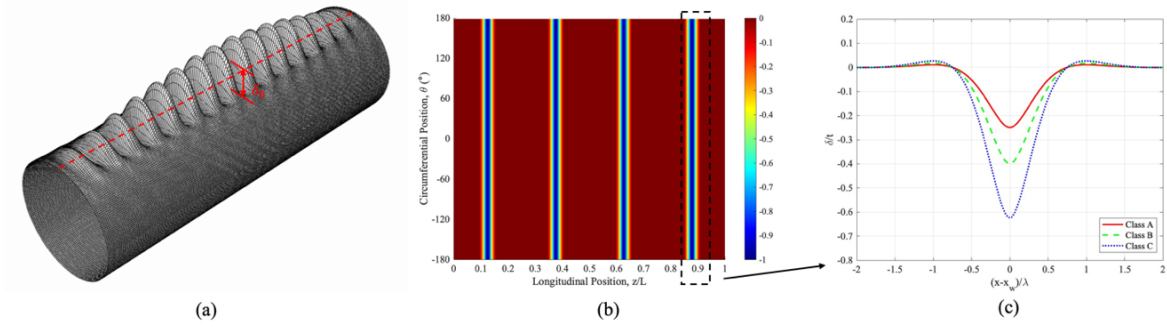


Figure 5: (a) First eigenmode-affine pattern under pure bending with the location of maximum imperfection δ_0 ; (b) specimens with scaled weld depression; (c) weld depression profile used in multiple models

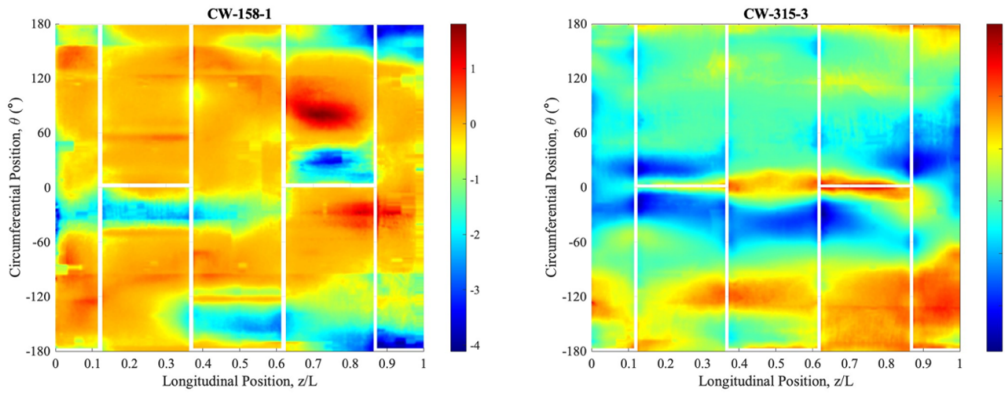


Figure 6: Scanned imperfections with removal of data around weld bead (Unit: mm)

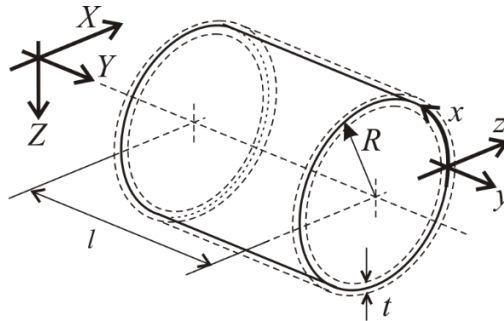


Figure 7: Illustration of coordinate system of tube used in Fourier series

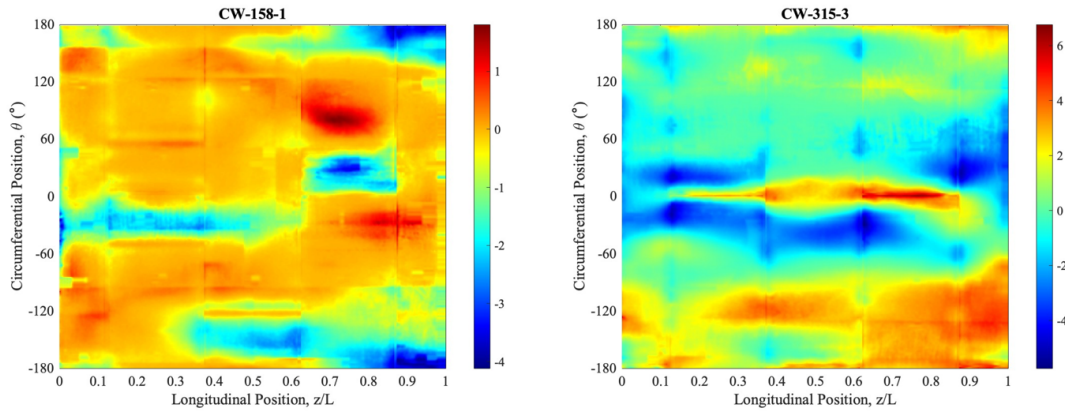


Figure 8: Scanned imperfections with area around weld bead filled with data generated by fitted Fourier series (Unit: mm)

5. Simulation results

5.1 Linear buckling analysis

Linear buckling analysis of the two specimens is performed in both ABAQUS and ANSYS. A reference moment of $1500 \text{ kN} \cdot \text{m}$ is applied for specimen CW-158-1 and $1000 \text{ kN} \cdot \text{m}$ for specimen CW-315-3. Comparison of the critical load factors predicted for the first eigenmode (α_{cr}) are provided in Table 6. Comparison of the eigen-buckling mode shape is provided in Fig. 9. Both in terms of eigenvalue and eigenmode ABAQUS and ANSYS results are comparable.

Table 6: Comparison of critical load factor calculated by ABAQUS and ANSYS

Specimen	Input moment ($\text{kN} \cdot \text{m}$)	α_{cr} (ABAQUS)	M_{cr} (ABAQUS)	α_{cr} (ANSYS)	M_{cr} (ANSYS)
CW-158-1	1500	5.187	7780	5.160	7740
CW-315-3	1000	1.939	1939	1.933	1933

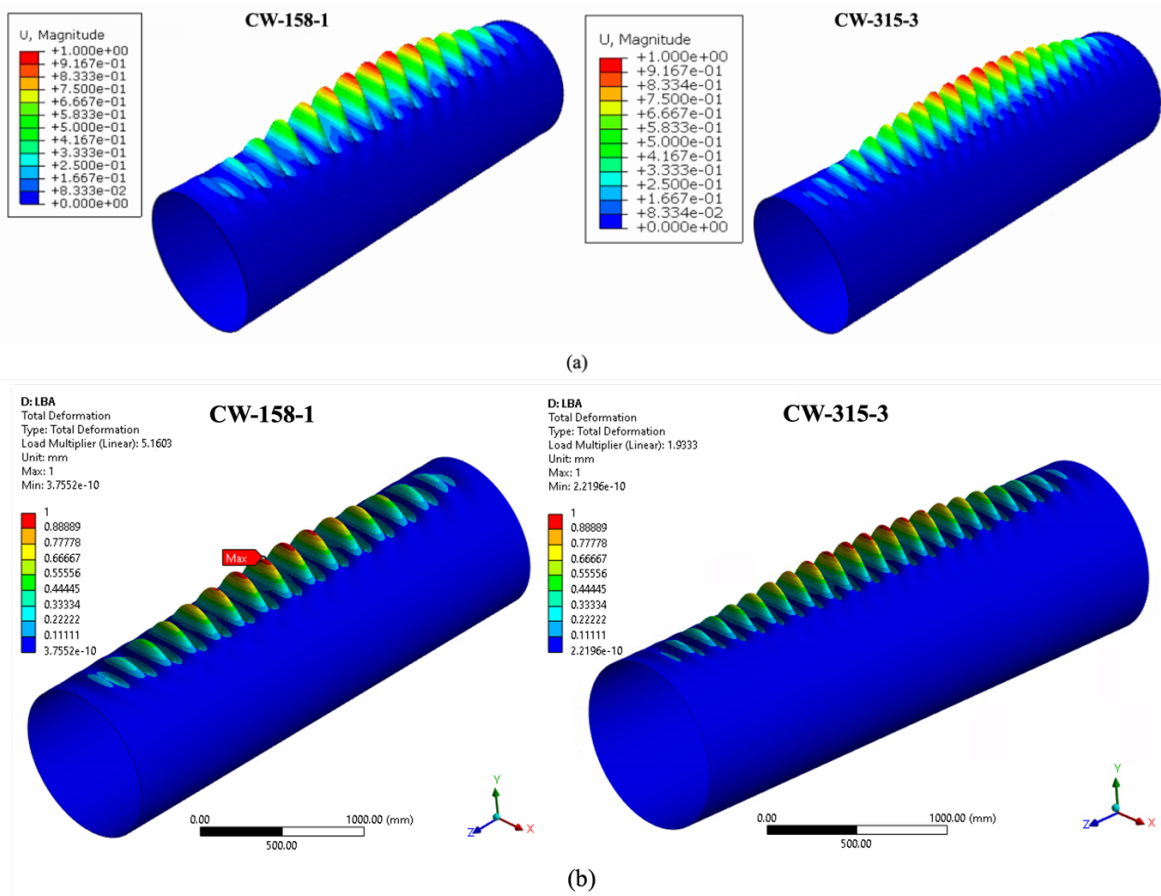


Figure 9: Comparison of first eigenmode generated by ABAQUS and ANSYS (a) ABAQUS; (b) ANSYS

5.2 Material nonlinear analysis

Material nonlinear analysis of the two specimens is performed in ABAQUS and ANSYS. The measured engineering stress-strain response assuming a proportional limit of $1.0f_y$ is converted to true stress-strain and the plastic strain provided as input to the models. The moment vs. total end rotation response is provided for the two models in Fig. 10 and the results are nearly identical.

Comparison of the fully material nonlinear (MNA) response to classical elastic first yield (M_y) and elastic-plastic (M_p) response is provided in Table 7, where:

$$M_y = \pi r^2 t f_y \quad (5)$$

$$M_p = 4r^2 t f_y \quad (6)$$

Two additional moments are also determined from the models and provided in Table 7: M_p^a and M_p^b , which provide the moment from the MNA analysis at which 5% equivalent plastic strain is observed. This MNA calculation allows for strain hardening and is reported at two levels: a) 5% surface strain, and b) 5% membrane strain. The shape factor for a thin cylindrical tube (i.e. Z/S or M_p/M_y) is $4/\pi \cong 1.27$, and the addition benefits to considering strain hardening are dependent on the stress-strain curve with a maximum increase of 1.15 over M_p for the first specimen, but only 1.08 over M_p for the second.

Table 7: Comparison of plastic load factor calculated with different strain assumption

Specimen	M_y (kN · m)	M_p (kN · m)	M_p^a (kN · m)	M_p^b (kN · m)	M_p^a/M_p	M_p^b/M_p
CW-158-1	2052	2613	3001	3010	1.15	1.15
CW-315-3	1034	1316	1422	1426	1.08	1.08

- a. Moment at which surface strain reaches 5% equivalent plastic strain
- b. Moment at which membrane strain reaches 5% equivalent plastic strain

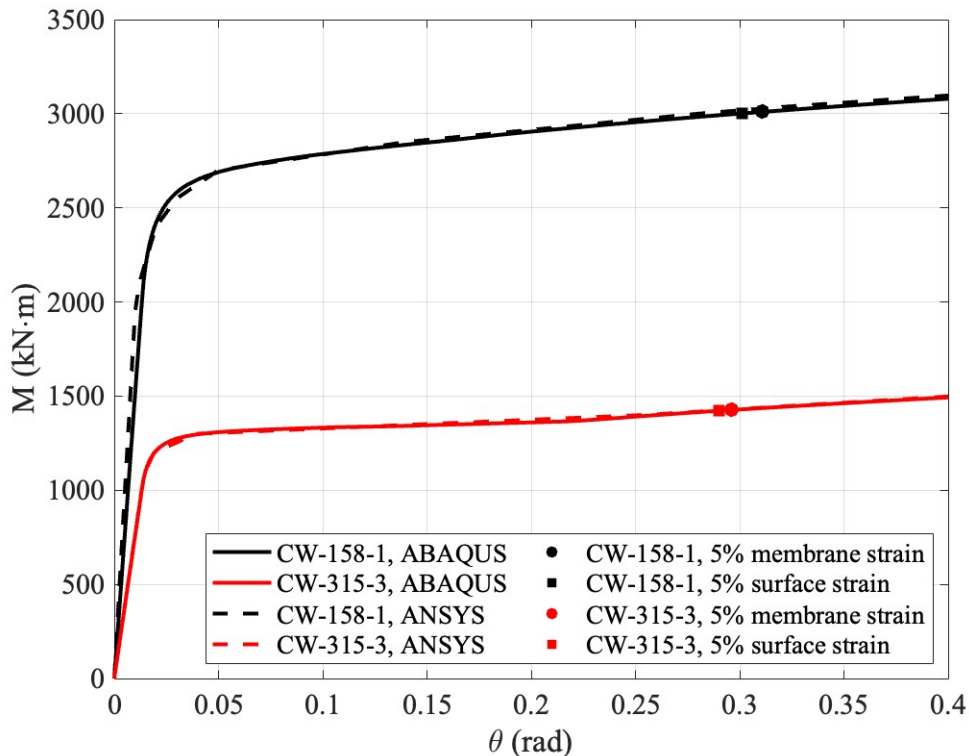


Figure 10: Comparison of Moment – rotation curve generated by ABAQUS and ANSYS for MNA

5.3 Geometrically and materially nonlinear analysis with imperfections included

GMNIA collapse simulations are conducted in both ABAQUS and ANSYS for the two specimens. The models have the same boundary conditions, mesh, material model, and imperfection patterns and magnitudes. (Note the eigen imperfections are independently generated in each solver, but as shown before are nearly identical). Both models use thin shell elements (S4R in ABAQUS and SHELL 181 in ANSYS), details of the elements may differ slightly, but the mechanics are nominally the same. In ABAQUS the Riks solver is employed, but the arc-length is not allowed to increase, and the model step sizes are such that at least 100 steps occur prior to reaching peak load. In ANSYS the Arclength method solver is employed, and step sizes are generally set to 0.02. Default convergence criteria and other solution controls are employed.

Results are provided for the three types of imperfections: first eigenmode-affine patterns, weld depression patterns, and scanned imperfections, and two choices of material proportional limit: $1.0f_y$ and $0.6f_y$. Peak moments from the models are summarized in Table 8 and moment vs. total rotation response is provided for eigenmode imperfections in Fig. 11, weld depression imperfections in Fig. 12, and scanned imperfections in Fig. 13. In general, both ABAQUS and ANSYS provide similar results, the weld depression is a more effective imperfection pattern in this loading condition than eigenmode imperfections, and scanned imperfection models show great promise, though are not a complete panacea to the challenges of GMNIA collapse modeling.

Table 8: Peak calculated moment from GMNIA simulations

Specimen	$M_{max,test}$ ($kN \cdot m$)	Imperfections type	Proportional limit	$M_{max,FE}$ ($kN \cdot m$)					
				ABAQUS			ANSYS		
				GMNIA EC3 classes			GMNIA EC3 classes		
				A	B	C	A	B	C
CW-158-1	1994	1st eigenmode	1.0fy	1856	1810	1777	1822	1730	1839
			0.6fy	1747	1697	1677	1778	1766	1728
CW-315-3	918		1.0fy	710	704	693	716	728	758
			0.6fy	693	686	682	699	708	740
CW-158-1	1994	Weld depression	1.0fy	2096	1984	1849	2090	1973	1850
			0.6fy	2081	1950	1796	2149	2075	1905
CW-315-3	918		1.0fy	844	758	664	899	821	724
			0.6fy	819	741	652	845	775	734
CW-158-1	1994	Scanned imperfections	1.0fy	2273			2335		
			0.6fy	2346			2353		
CW-315-3	918		1.0fy	889			865		
			0.6fy	837			801		

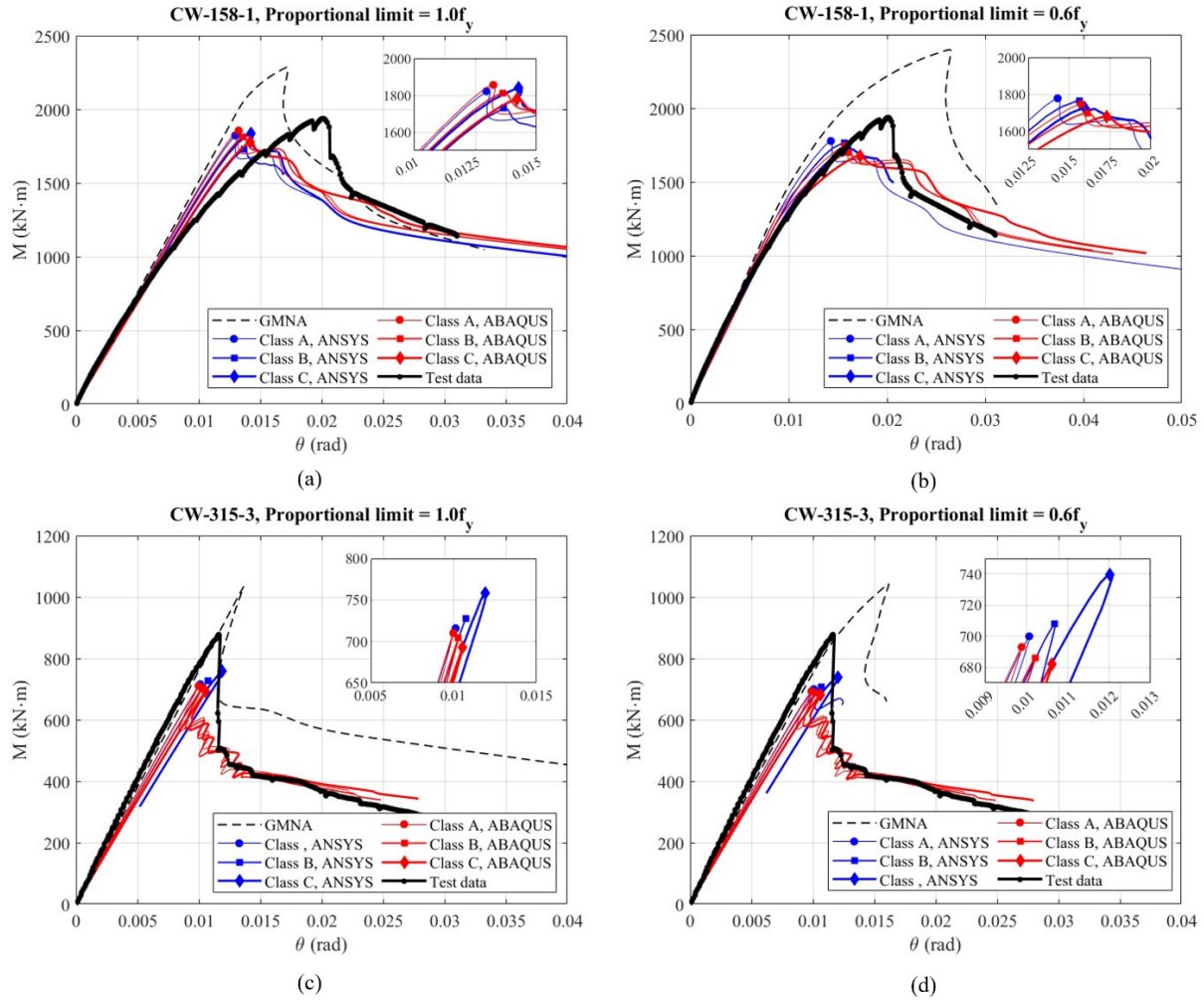


Figure 11: Comparison of Moment – rotation curve generated by ABAQUS and ANSYS for GMNIA using first eigenmode imperfections

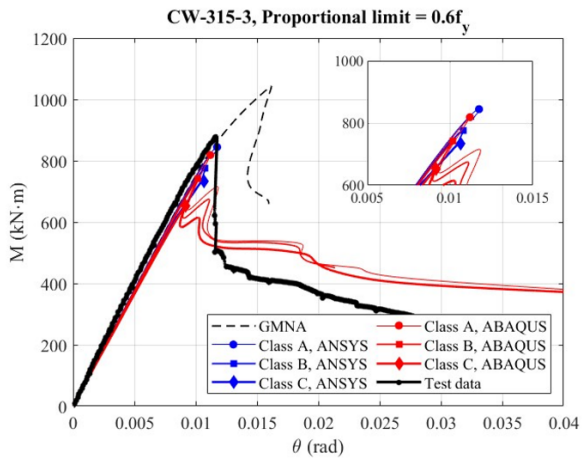
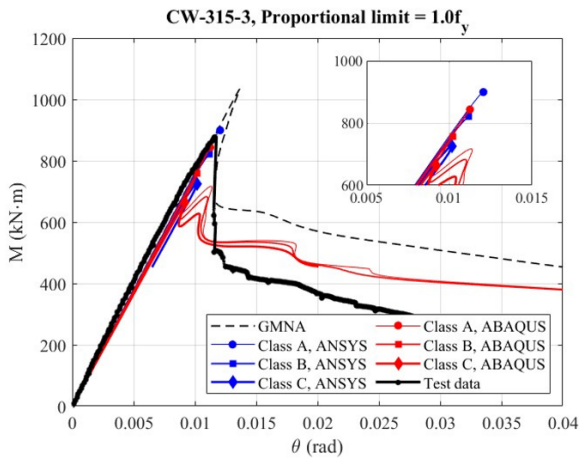
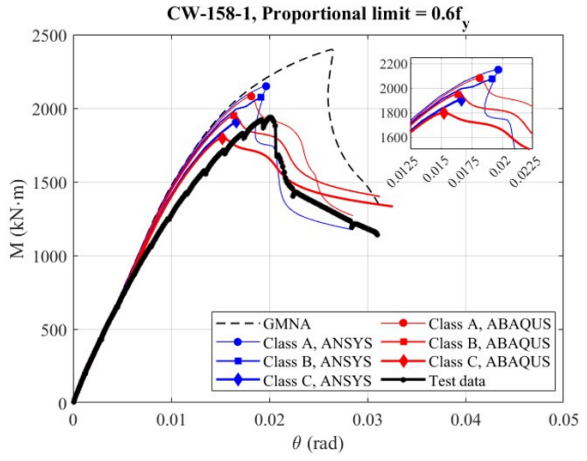
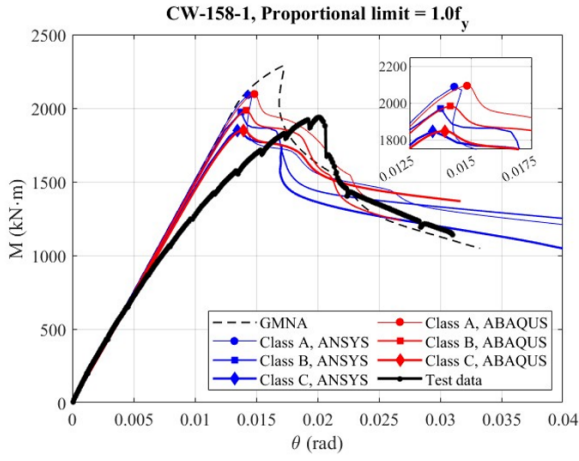


Figure 12: Comparison of Moment – rotation curve generated by ABAQUS and ANSYS for GMNIA using weld depression

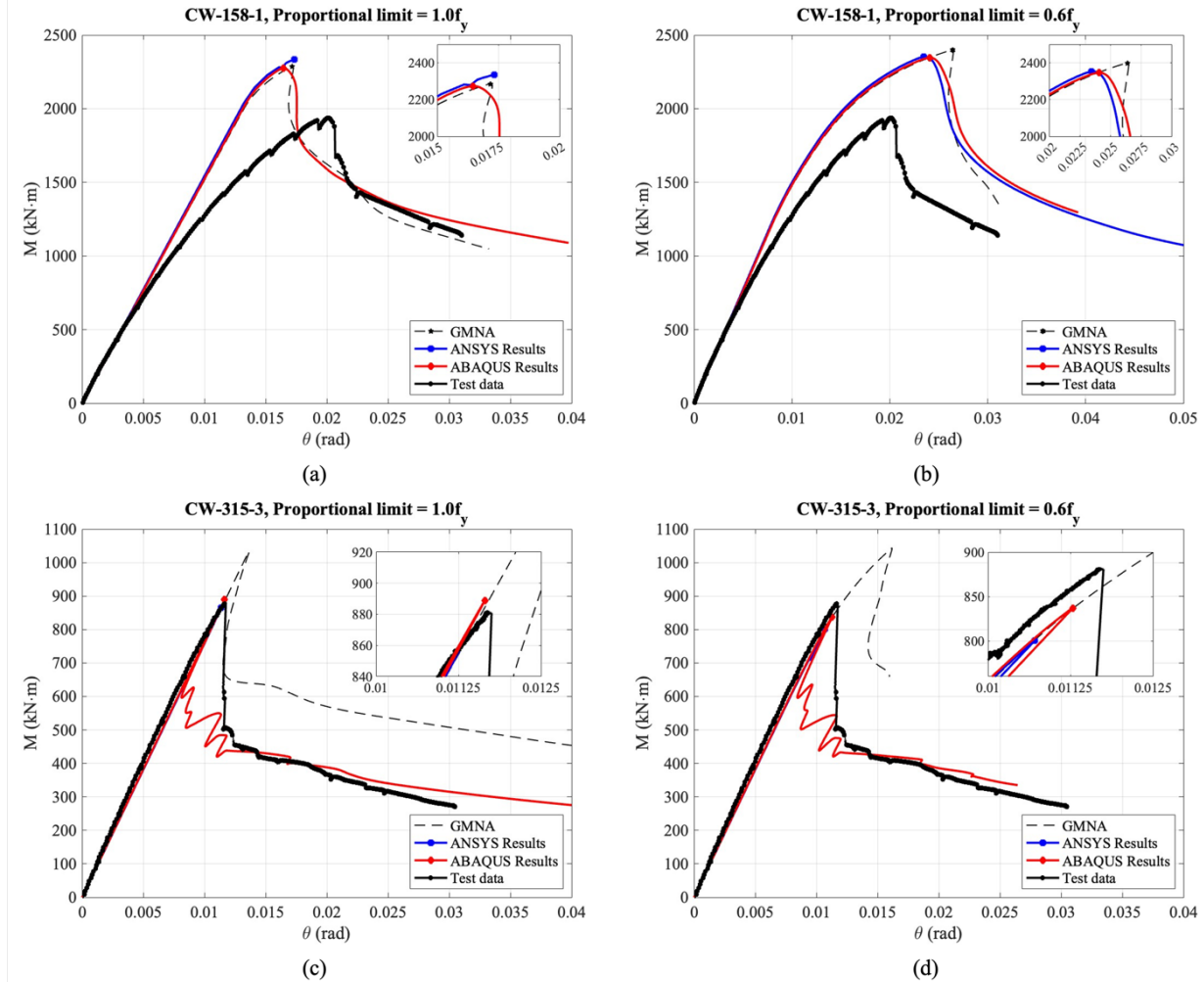


Figure 13: Comparison of Moment – rotation curve generated by ABAQUS and ANSYS for GMNIA using scanned imperfections

GMNIA simulations with eigenmode imperfections are in poor agreement with tested capacity. In addition, the eigenmode imperfections models exhibit little sensitivity to imperfection magnitude (i.e. quality class). In comparing the ABAQUS and ANSYS results the ABAQUS results exhibit greater consistency – larger imperfections always generate smaller peak moments. While ABAQUS and ANSYS have excellent agreement with the LBA and MNA, the GMNIA equilibrium paths especially for the CW-158-1 specimen with the $0.6f_y$ proportional limit, differ – with ABAQUS consistently predicting softer overall response than in the ANSYS model.

GMNIA simulations with weld depression imperfections show greater strength sensitivity to imperfection magnitude, particularly for the stockier CW-158-1 specimen. In addition, the simulation strengths agree more closely with the tested capacity and assumed imperfection / quality class. This result is consistent with the recommendations of Wang et al. (2020). As with the eigenmode imperfection solutions, ABAQUS peak moments again show greater numerical consistency than the ANSYS results. In the process of performing and comparing the results we observed that the ANSYS solution was particularly sensitive to the arc-length step size, particularly in the primarily elastic Class A imperfection CW-315-3 specimen. For the slender

CW-315-3 specimen ANSYS results are consistently higher in predicted strength than ABAQUS, in the most extreme case, 12% higher.

GMNIA simulations with scanned imperfections show reasonable agreement with tested response. For the slender tubes (CW-315-3) the agreement is excellent in terms of strength, with an error of 3%, as well as overall response as shown in Fig. 13. However, for the stockier tube (CW-158-1), the strength is 10% higher than the tested capacity and the moment-rotation response is not in good agreement near peak load. It is hypothesized that this model is particularly sensitive to weld depressions (as demonstrated in the results of Fig. 12). The method used to fill in the missing imperfection data at welds (customized Fourier series) does not especially account for weld depressions and it is hypothesized that this may be a source of error in this model. Scanning from the inside, or more direct use of the weld depression function fit to the available data are two possible solutions to remediate this lack of agreement.

6. Discussion

Utilization of GMNIA collapse analysis in the structural design of cylindrical wind turbine support towers holds great promise for improving efficiency and directly connecting manufacturing quality to reliability of installed towers. The benchmark testing utilized herein, demonstrates some of the challenges with developing a robust and reliable GMNIA modeling protocol, even for a tube under a single action. With care taken on boundary conditions, element selection, mesh, and material model then LBA and MNA models are shown to be robust and consistent across the most popular commercial finite element packages. However, even with this care extended to the modeling of geometric imperfections, the sensitivity of the simulation reveals sensitivities to solver assumptions and some disagreement between the solutions generated from ABAQUS and ANSYS shell finite element models. Significant work remains to explore the results across a greater body of benchmarks, to more fully explore the solvers, solver inputs, and convergence criteria, and ultimately to provide definitive modeling guidance.

7. Conclusions

Wind turbine support towers rely on thin-walled steel cylinders that are highly sensitive to imperfections. The tower manufacturing process utilizing “can-welding” introduces important geometric imperfections to the formed tube. Geometric and material nonlinear analysis with imperfections (GMNIA) with shell finite element models holds promise as a robust method to reliably predict the strength of these tubes. However, sensitivity to the assumed geometric imperfections, fidelity in which the material model is realized, and even the finite element package utilized, e.g. ABAQUS or ANSYS all have a potential role to play in the predicted response. Two recently conducted flexural tests on 1 m diameter steel tubes, one reasonably stocky and the other quite slender, which were carefully scanned for initial geometry, are utilized as benchmarks in a numerical study of structural response. Both ABAQUS and ANSYS models, with similar modeling protocols, are conducted for the tubes, and excellent agreement is shown in isolated linear buckling analysis and material nonlinear analysis. However, when conducting GMNIA collapse simulations significant sensitivity to the imperfection assumptions, and in some cases the solvers employed, is demonstrated. The inadequacy of using the first eigen-buckling mode as the imperfection pattern is demonstrated. While significant efforts were made to utilize the laser-scanned imperfections in the models, additional work remains, as the external scans of the tubes do not provide critical information about weld depression imperfections, due to the presence of

the weld bead. In the case of the slenderest tube tested the scanned imperfection pattern did provide excellent results in comparison to tested response. Additional work remains to develop a robust set of modeling and solver protocols for GMNIA collapse modeling of wind turbine support towers.

Acknowledgments

The authors would like to acknowledge Victoria Ding and Ziqi Tang who contributed to discussions on this work. This paper is based upon work supported by the National Science Foundation under grants CMMI-1334489 and CMMI-1334122. Any opinions, findings, and conclusions or recommendations expressed in this material are those of the author(s) and do not necessarily reflect the views of the National Science Foundation.

References

- Berry, P. A., Rotter, J. M., & Bridge, R. Q. (2000). "Compression tests on cylinders with circumferential weld depressions." *Journal of engineering mechanics*, 126(4), 405-413.
- CEN (European Committee for Standardization). (2007). "Design of steel structures. Part 1-6: Strength and stability of shell structures." EN 1993-1-6, Eurocode 3, Brussels, Belgium.
- Jay, A., Myers, A. T., Mirzaie, F., Mahmoud, A., Torabian, S., Smith, E., & Schafer, B. W. (2016a). "Large-scale bending tests of slender tapered spirally welded steel tubes." *Journal of Structural Engineering*, 142(12), 04016136.
- Jay, A., Myers, A. T., Torabian, S., Mahmoud, A., Smith, E., Agbayani, N., & Schafer, B. W. (2016b). "Spirally welded steel wind towers: Buckling experiments, analyses, and research needs." *Journal of Constructional Steel Research*, 125, 218-226.
- Lantz, E. J., Roberts, J. O., Nunemaker, J., DeMeo, E., Dykes, K. L., & Scott, G. N. (2019). "Increasing wind turbine tower heights: Opportunities and challenges."
- Lin, D., Pervizaj, A., Madsen, S.B., Myers, A. (2024) "Flexural buckling tests on 1:4 scale wind turbine tower tubes." *Structural Stability Research Council Annual Stability Conference*, March 2024, San Antonio, TX
- Mahmoud, A., Mirzaie, F., Torabian, S., Jay, A., Myers, A. T., Smith, E., & Schafer, B. W. (2016). "Collapse analysis of spirally welded tapered tubes under flexural moments using measured and generated imperfections." *In Proc., 7th Int. Conf. on Coupled Instabilities in Metal Structures, CFSRC-Johns Hopkins Univ.*, Baltimore.
- Mahmoud, A. (2017). "Analysis and Design of Spirally Welded Thin-Walled Steel Tapered Cylindrical Shells Under Bending with Application to Wind Turbine Towers" (Doctoral dissertation, Johns Hopkins University).
- Mahmoud, A., Torabian, S., Jay, A., Mirzaie, F., Myers, A. T., Smith, E., & Schafer, B. W. (2018). "Modeling the flexural collapse of thin-walled spirally welded tapered tubes." *Journal of Structural Engineering*, 144(2), 04017201.
- Rotter, J. M., & Teng, J. G. (1989). "Elastic stability of cylindrical shells with weld depressions." *Journal of Structural Engineering*, 115(5), 1244-1263.
- Rotter, J. M., and Schmidt, H. (2013). *Buckling of steel shells European design recommendations*, 5th Ed., ECCS Press, Brussels, Belgium.
- Sadowski, A. J., Seidel, M., Al-Lawati, H., Azizi, E., Balscheit, H., Böhm, M., ... & Zhang, P. (2023). "8-MW wind turbine tower computational shell buckling benchmark. Part 1: An international 'round-robin' exercise." *Engineering Failure Analysis*, 148, 107124.
- Sadowski, A. J., & Seidel, M. (2023). "8-MW wind turbine tower computational shell buckling benchmark. Part 2: Detailed reference solution." *Engineering Failure Analysis*, 148, 107133.
- Sadowski, A. J., Morata, M. T., Kathirkamanathan, L., Seidel, M., & Rotter, J. M. (2023). "On the existing test dataset of isotropic cylindrical metal shells under axial compression and the design of modern metal civil engineering shells." *Structural Safety*, 102, 102285.
- Wang, J., Fajuyitan, O. K., Orabi, M. A., Rotter, J. M., & Sadowski, A. J. (2020). "Cylindrical shells under uniform bending in the framework of Reference Resistance Design." *Journal of Constructional Steel Research*, 166, 105920.